

Neuroanatomy and Neurochemistry of Mouse Cornea

Jiucheng He¹⁻³ and Haydee E. P. Bazan¹⁻³

¹Louisiana State University Health, School of Medicine, New Orleans, Louisiana, United States

²Neuroscience Center of Excellence, Louisiana State University Health, New Orleans, Louisiana, United States

³Department of Ophthalmology, Louisiana State University Health, New Orleans, Louisiana, United States

Correspondence: Haydee E. P. Bazan, Department of Ophthalmology and Neuroscience Center of Excellence, Louisiana State University Health, 2020 Gravier Street, Suite D, New Orleans, LA 70112, USA; hbazan1@lsuhsc.edu.

Submitted: August 21, 2015

Accepted: November 30, 2015

Citation: He J, Bazan HEP. Neuroanatomy and neurochemistry of mouse cornea. *Invest Ophthalmol Vis Sci.* 2016;57:664-674. DOI:10.1167/iops.15-18019

PURPOSE. To investigate the entire nerve architecture and content of the two main sensory neuropeptides in mouse cornea to determine if it is a good model with similarities to human corneal innervation.

METHODS. Mice aged 1 to 24 weeks were used. The corneas were stained with neuronal-class β III-tubulin, calcitonin gene-related peptide (CGRP), and substance P (SP) antibodies; whole-mount images were acquired to build an entire view of corneal innervation. To test the origin of CGRP and SP, trigeminal ganglia (TG) were processed for immunofluorescence. Relative corneal nerve fiber densities or neuron numbers were assessed by computer-assisted analysis.

RESULTS. Between 1 and 3 weeks after birth, mouse cornea was mainly composed of a stromal nerve network. At 4 weeks, a whorl-like structure (or vortex) appeared that gradually became more defined. By 8 weeks, anatomy of corneal nerves had reached maturity. Epithelial bundles converged into the central area to form the vortex. The number and pattern of whorl-like structures were different. Subbasal nerve density and nerve terminals were greater in the center than the periphery. Nerve fibers and terminals that were CGRP-positive were more abundant than SP-positive nerves and terminals. In trigeminal ganglia, the number of CGRP-positive neurons significantly outnumbered those positive for SP.

CONCLUSIONS. This is the first study to show a complete map of the entire corneal nerves and CGRP and SP sensory neuropeptide distribution in the mouse cornea. This finding shows mouse corneal innervation has many similarities to human cornea and makes the mouse an appropriate model to study pathologies involving corneal nerves.

Keywords: corneal innervations, mouse cornea, trigeminal ganglia, substance P, calcitonin gene-related protein

There has been a renewed interest in studying corneal nerves in recent years, due in part to the fact that corneal nerves are routinely injured after refractive surgical procedures and to the recognition that corneal innervation plays a central role in the maintenance of a healthy ocular surface.¹⁻¹⁰ Several animal models have been used for studying corneal neurobiology.⁶⁻¹⁶ Of these models, the mouse is the most popular because it is relatively inexpensive, easy to reproduce, and because animals reach adulthood quickly compared with other models. An important advantage is that mice can be genetically manipulated, and there is an extensive array of antibodies that are reactive to mouse tissues. In addition, 99% of the genes are equivalent to those in humans,¹⁷ making mice ideal for studying the function of human genes as well as specific diseases.

Several groups have used immunochemical methods to study mouse corneal innervation,^{14-16,18,19} but none of them have provided an entire map of its innervation or the content of the most abundant neuropeptides, calcitonin gene-related peptide (CGRP), and substance P (SP). A transgenic mouse expressing neuro-specific yellow fluorescent protein (YFP) has been used for studying nerve regeneration.²⁰ It has proven to be a good model for visualization of corneal nerves in vivo and could provide a whole-mount view of the entire corneal innervation.²¹⁻²³ However, only half of the subbasal nerves in this mouse model are YFP-labeled.²⁰ Using a modified method of immunofluorescence and imaging developed in our labora-

tory,²⁴⁻²⁸ we characterize the whole corneal nerve architecture of the mouse from early postnatal age to adulthood in this study. We also investigate the distribution of the main sensory neuropeptides CGRP and SP.

METHODS

Animals

Fifty-four Swiss Webster mice aged 1 to 24 weeks (both sexes) were purchased from Charles River Laboratories (Wilmington, MA, USA) and housed at the Neuroscience Center of Excellence, Louisiana State University Health (LSUH; New Orleans, LA, USA). The animals were handled in compliance with the guidelines of the ARVO Statement for the Use of Animals in Ophthalmic and Vision Research, and the experimental protocol was approved by the Institutional Animal Care and Use Committee at LSUH.

Antibodies

Rabbit monoclonal anti- β III-tubulin (Tuji1, MRB-435p-100) antibody was purchased from Covance Antibody Services, Inc. (Berkeley, CA, USA); rat monoclonal anti-substance P (SP) was purchased from Millipore (Temecula, CA, USA); and guinea pig polyclonal anti-CGRP was purchased from Pierce Antibody



Products (Thermo Fisher Scientific, Inc., Rockford, IL, USA). Secondary antibodies AlexaFluor 488 goat anti-rabbit IgG (H+L), AlexaFluor 594 goat anti-guinea pig IgG (H+L), and AlexaFluor 594 goat anti-rat IgG (H+L) were purchased from Invitrogen (Carlsbad, CA, USA).

Immunofluorescence Staining and Imaging

Mice were anesthetized by an intraperitoneal injection of 0.1 mL sodium pentobarbital (10 mg/mL). The position of the cornea was marked by three stitches at 3, 9, and 12 o'clock points with a nylon 10-0 monofilament (Ethilon; Ethicon, Inc., Somerville, NJ, USA) on the sclerocorneal rim. The mice were euthanized and the eyeballs were enucleated and fixed in freshly prepared 2% paraformaldehyde for 15 minutes. Then the corneas were carefully excised along the sclerocorneal rim and fixed for an additional 45 minutes, followed by three washes with 0.1 M PBS containing 0.1% bovine serum albumin (PBS-BSA). To block nonspecific binding, corneas were placed in a 96-well plate (one cornea/well) and then incubated with 10% normal goat serum plus 0.3% Triton X-100 solution in PBS-BSA for 60 minutes at room temperature. The tissue was then incubated with rabbit monoclonal anti- β III-tubulin antibody (1:1000) for 72 hours at 4°C. After washing with PBS-BSA (3 \times 10 minutes), the corneas were incubated with the corresponding secondary antibodies for 24 hours at 4°C and then washed thoroughly with PBS-BSA.

For double immunofluorescence, after labeling with the first set of antibodies (β III-tubulin and corresponding secondary antibodies) was completed, the tissue was incubated with a second primary antibody (CGRP or SP) for 72 hours and followed by the corresponding fluorescein isothiocyanate (FITC)- or tetramethylrhodamine (TRITC)-conjugated secondary antibody and washings, as described above.

Four radial cuts were performed on each cornea, and the tissue was flatly mounted on a slide with the endothelium side up. Images were acquired in time-lapse mode using a fluorescence microscope (Nikon Eclipse TE200; Nikon Corp., Tokyo, Japan) equipped with a digital camera (CoolSNAP HQ; Photometrics, Tucson, AZ, USA) using imaging software (MetaVue; Molecular Devices, Sunnyvale, CA, USA). The images of mice of different ages (Fig. 1) were taken with a fluorescent microscope (Olympus IX71; Olympus Corp., Tokyo, Japan). The images at the same layer recorded from one cornea were merged together to build an entire view of the corneal nerve network of both the epithelium and stroma. To obtain a transected view of the corneal nerves, the same cornea used above was embedded in optimal cutting temperature (OCT), and serial 15- μ m cryostat sections were cut and photographed with the same microscope.

To test the origin of the sensory neuropeptides CGRP and SP, mice were euthanized, the crania opened, and both left and right TG removed and processed as previously described.²⁸ Briefly, after fixing and washing the tissue, the whole TG were embedded in OCT compound and serial 10- μ m cryostat sections were cut, dried at room temperature for 2 hours, and stored at -20°C until use.

For double immunofluorescence, the sections of the TG were washed, blocked, and permeabilized as already described²⁸ and then incubated with primary antibodies against β III-tubulin (1:1000) plus CGRP (1:500), β III-tubulin plus SP (1:500), or CGRP plus SP in 0.1 M PBS containing 1.5% normal goat serum overnight at 4°C. After washing with PBS-BSA (3 \times 5 minutes), the sections were incubated with corresponding FITC- or TRITC-conjugated secondary antibodies for 1 hour at room temperature. To exclude nonspecific labeling, the primary antibodies were replaced by serum IgG of the same

host species as the primary antibody. In controls without primary antibodies, there was no staining (data not shown).

Data Analysis

The adult mouse corneas (22 mice) have a radius of approximately 1.5 mm. To calculate the subbasal epithelial nerve densities, we divided the mouse cornea into central and peripheral zones. The central zone was defined by a radius of 0.5 mm starting at the apex, and the peripheral zone with a radius of 0.5 mm beginning at the limbus. To avoid overlap, approximately 0.5 mm of space between the two zones was left uncounted.

To get a better contrast, the fluorescent images were changed to grayscale mode and placed against a white background using imaging software (Photoshop; Adobe Systems, Inc., Mountain View, CA, USA). The subbasal nerve fibers in each image were carefully drawn with 4-pixel lines following the course of each fiber by using the brush tool in the imaging software (Adobe Systems, Inc.). The nerve area and the total area of the image were obtained by using the histogram tool. The percentage of total nerve area was quantified for each image as described previously.²⁵⁻²⁸ To compare nerve densities in the central and peripheral areas, eight images for each zone were randomly chosen from each cornea (two images/quadrant). A total of 80 images for each zone from 10 corneas of 10 mice (5 mice/sex) were averaged. Nerve terminals in the superficial epithelia within the central and peripheral zones were calculated by directly counting the number of terminals in each image. Twenty-four images per zone from six corneas were analyzed. The terminal numbers in each image were counted directly. Since each image comprised an area of 0.335 mm², the terminal numbers per square millimeter were calculated.

To examine the relative content of neuropeptides in the subbasal nerves, 12 corneas that had been stained with anti- β III-tubulin were double-stained with CGRP or SP. For each neuropeptide, a total of 24 whole-mount images from the central zone (one image/quadrant) were taken, and then the same numbers of images were taken for β III-tubulin. In the same visual field, the percentage of β III-tubulin equaled that of the total nerve area, and the ratio of the peptide-positive nerve area against β III-tubulin represented the relative content.

To calculate CGRP- and SP-positive neurons in the TG, 20 images were selected randomly from 10 mice (1 section/ganglion) and counted in a blind fashion. Differences in central and peripheral corneal nerve densities, terminal numbers, and the relative content of neuropeptides in the central cornea and TG were expressed as means \pm SEM and *t*-test was performed; *P* < 0.05 was considered a statistically significant difference between two groups.

RESULTS

Development of Mouse Corneal Innervation After Birth

When comparing the subbasal epithelial nerve densities in corneas of adult male and female mice (*n* = 10 corneas/sex), no differences in epithelial nerve densities were found between sexes either in the central or in the peripheral epithelial nerves (data not shown). Therefore, the data presented represent a combination of both sexes. For this study, a total of 32 mice were used, with four mice for each time point.

Figure 1 contains representative images of corneal stroma and epithelial nerves from mice 1 to 24 weeks after birth. Images were recorded with a \times 10 objective lens focusing on

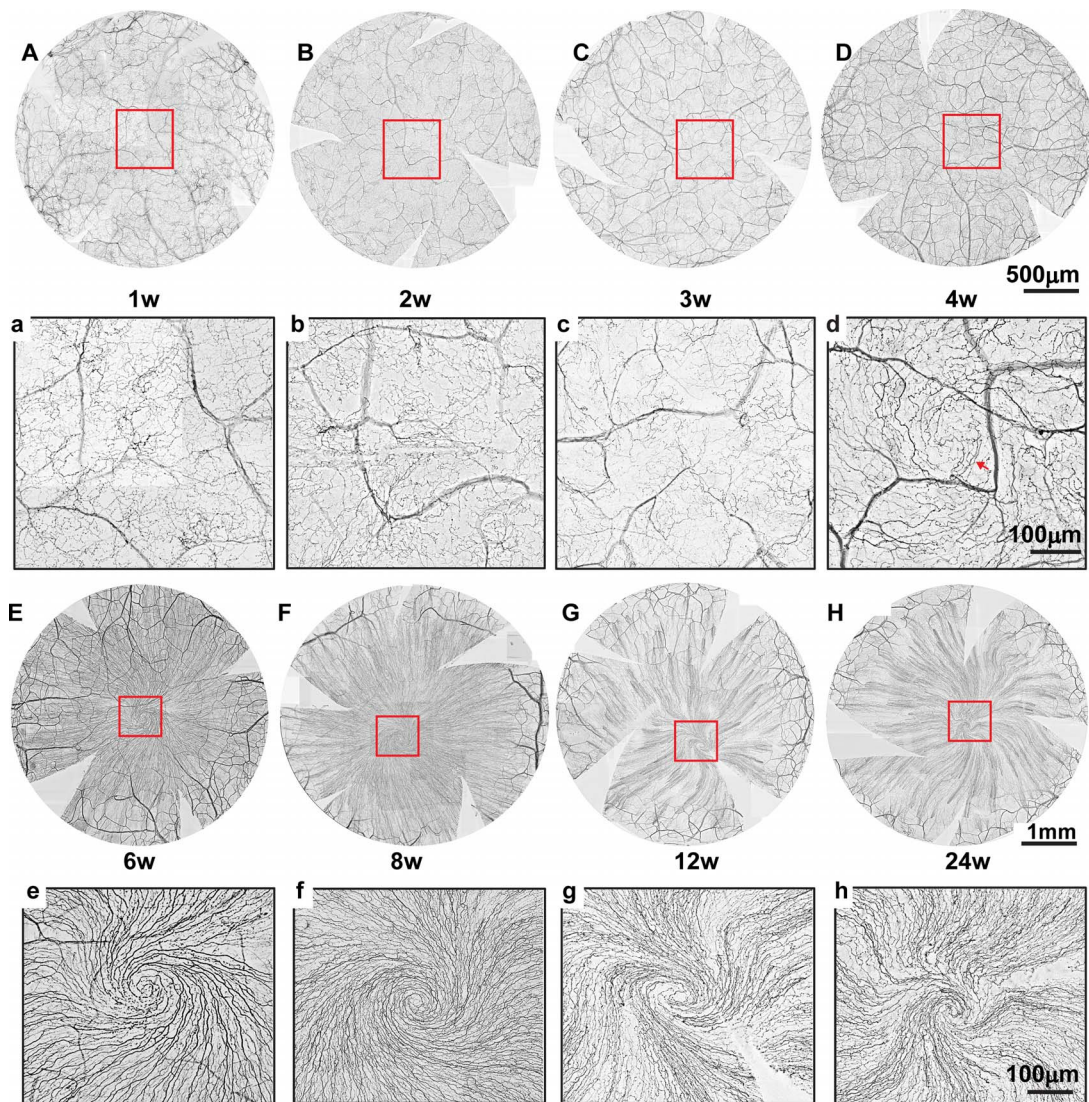


FIGURE 1. Development of mouse corneal stromal and epithelial innervation after birth. Images in (A–H) show representative whole mounts of entire corneal innervation from 32 mice aged 1 to 24 weeks (4 mice/time point). Highlighted images in (A–H) are close-ups showing the detailed structures of corneal nerves in the central area as framed in (A–H). *Arrow* in (D) indicates the whorl-like structure. Corneas were labeled with anti- β III-tubulin antibody and images taken with a fluorescent microscope (Olympus Corp.) and with a $\times 10$ objective lens.

the subbasal layer. In the very young mice (aged between 1 and 3 weeks), the more prominent nerves were the thick stromal nerves, which connected with each other, constituting a dense stromal nerve network. There was little change in the size of the stromal nerve bundles between the periphery and center. Subbasal nerves originating from the branches of stromal nerves were few, short and thin, as can be seen in the images (Figs. 1A–D) depicting the central area of the cornea. Whorl-like structures started forming at 4 weeks. From age 4 to 6 weeks, the density and branches of the corneal stromal nerves in the central cornea were gradually reduced (compare Figs. 1A–D with Fig. 1E), and the subbasal nerve bundles became longer. By age 8 weeks, the mouse corneal innervation reached maturity. The stromal nerves looked like a tree; their trunks around the limbal area were thicker, but their branches became gradually thinner from the corneal periphery to the center, in which a few stromal nerve branches were visible. On the contrary, the subbasal nerves, which mainly originated from the peripheral stromal nerves, were much longer and thicker. From 8 to 24 weeks, the vortex was well defined (Figs. 1F–H)

and there were no obvious changes in the epithelial nerve architecture.

Corneal Nerve Architecture of Adult Mice

Stromal Nerves. The stromal nerves originate from four major nerve trunks, which pass through the attachment points of extraocular muscles and run from the episclera to the corneoscleral limbus, where they divide into several branches. A reconstructed image in Figure 2A shows the fiber course of a medial (nasal) nerve trunk in an 8-week-old mouse. Some of the stromal branches connected with each other to constitute a dense stromal nerve network around the limbal area, but most of the branches run forward and divide further into many subbranches. In the peripheral zone, these branches run upward to the subbasal layer to give place to subbasal bundles. Figure 2B shows the entire whole-mount view of stromal nerves recorded from two mouse eyes. There was an average of 21.7 ± 0.8 ($n = 20$ eyes, means \pm SEM) branches per eye, and based on qualitative observations, the density of the stromal nerves was higher in the periphery than in the center.

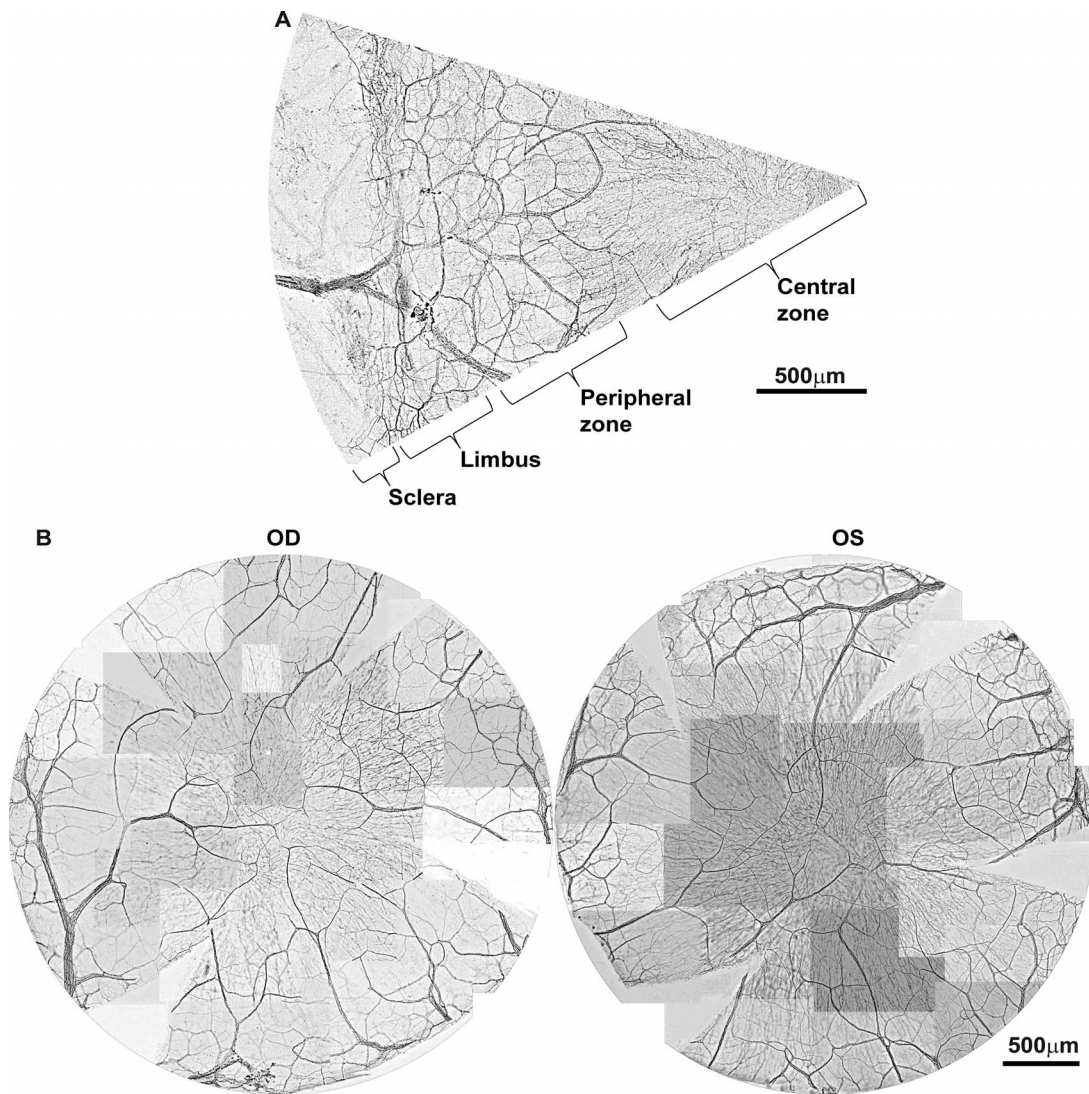


FIGURE 2. The origin and distribution of corneal stromal nerves. Mouse corneal nerves originate from four major nerve trunks that run through the attachments of extraocular muscles to the limbus, where they divide repeatedly into many branches. The branches connect with each other and constitute a stromal nerve network. In adult mice (8 weeks), the density of stromal nerves is higher in the periphery than that in the center. (A) Reconstructed image showing the nerve course of a nasal major nerve trunk. (B) Reconstructed whole-mount images showing the entire view of the stromal nerve architectures recorded from two eyes of a mouse. Corneas were labeled with anti- β III-tubulin antibody and images were recorded with a $\times 10$ objective lens, focusing on the subbasal layer.

Epithelial Nerves. Figure 3A shows the whole mount of the entire subbasal nerves recorded from the same mouse as in Figure 2B. The epithelial nerves emerge mainly from the tips of the stromal nerve branches in the periphery and form the nerve bundles in the subbasal layer. Long bundles run from the periphery and converge into the central area to form the whorl-like structure or vortex. These subbasal bundles project numerous divisions that connect to each other to constitute the subbasal nerve plexus. Fine terminals or free endings derivate from the plexus and innervate the epithelial cells (Fig. 3B). Highlighted images in Figure 3C show the detailed nerve architecture of stromal nerves, subbasal bundles, and nerve terminals at the vortex area.

One interesting finding was that the patterns and numbers of whorl-like structures varied between corneas of 8-week-old mice (Fig. 3A). Among the 60 corneas analyzed, 44 (73.3%) showed one whorl-like structure per cornea, and 28 of those eyes had a clockwise pattern, as shown in Figure 3A (right eye), while the other 16 eyes had a counterclockwise pattern

(Fig. 3A, left eye). Eleven eyes (18.3%) showed two whorl-like structures, as represented in Figure 3C (left eye, arrows); in two eyes (3.3%), we observed three whorl-like structures (Fig. 4). Three other eyes (5%) did not present these structures, but instead contained long bundles running across the central area and merging in the inferior-nasal corneoscleral area. Furthermore, among the 30 mice analyzed, 18 mice showed one whorl-like structure in both eyes; seven mice showed one whorl-like structure in one eye and two such structures in another eye. One mouse showed two vortexes in both eyes, and two mice showed one cornea with two whorl-like structures and three vortexes in the other cornea.

The montage of the corneal sagittal sections labeled with β III-tubulin antibody showed the cross-sectional view of the whole corneal innervation (Fig. 5). Highlighted images from the center and periphery depict the detailed distribution of nerve terminals in the epithelia, revealing that the density of epithelial terminals was higher in the center than in the periphery.

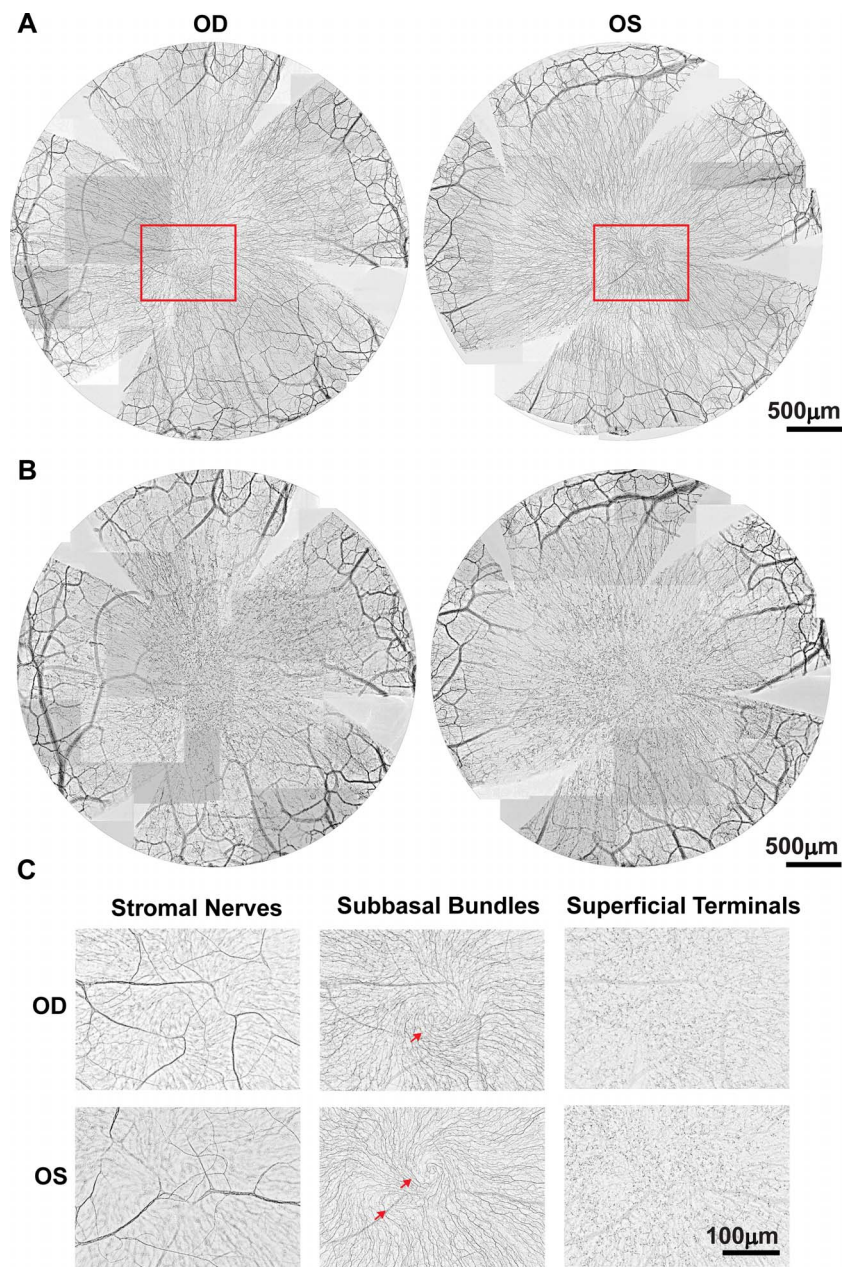


FIGURE 3. Epithelial nerve architecture of mouse cornea. The epithelial nerves derive from the stromal nerve branches that penetrate to the subbasal layer and give place to the subbasal bundles. In adult mouse corneas (8 weeks), the penetrating sites were located mainly in the peripheral zone, and it was generally found that one penetrating site gives origin to several nerve bundles. Those bundles run centripetally and converge into the central area to form the whorl-like structure or vortex. The patterns and number of vortices differ among the eyes. These main bundles divided into branches, which connect to the bundles to form the subbasal nerve network. Fine terminals bud from the network to innervate the epithelial cells. (A, B) Whole-mount images of the entire architecture; (A) focuses on the corneal subbasal nerves and (B) focuses on the superficial free endings recorded from the same mouse shown in Figure 2B. (C) Highlighted images, as framed in (A), show the detailed nerve architectures in the vortex area. *Arrows* indicate the whorl-like structures. It is noteworthy that in the same mouse, the left eye has two vortices that go in opposite directions.

The density of subbasal nerves and nerve terminals in the mouse cornea were recorded from 10 corneas, as explained in the Methods section. The subbasal nerve density, calculated as the percentage of total area, was $28.2\% \pm 0.3\%$ in the central area and $18.1\% \pm 0.4\%$ in the peripheral area (Figs. 6A, 6B), with a significant difference of $P < 0.001$. Similarly, nerve terminals, calculated from 48 images (24 images per zone) of 6 eyes as the average number of terminals/mm² were also greater in the center (3972 ± 58) than in the periphery (1976 ± 99 , $P < 0.001$, Figs. 6C, 6D).

CGRP and SP Content of Mice Corneal Nerves

Whole corneas labeled with β III-tubulin were double stained with antibodies against CGRP or SP. Representative images of mouse subbasal nerve bundles in the vortex area, terminals, and stromal trunks are shown in Figures 7A and 7B.

In the central zone, CGRP-positive nerve fibers constituted $70.2\% \pm 2.4\%$ of the total subbasal nerve content, while SP-positive nerves were $58.6\% \pm 1.4\%$ ($n = 6$ eyes; $P < 0.0001$). The percentage of CGRP-positive terminals was also higher

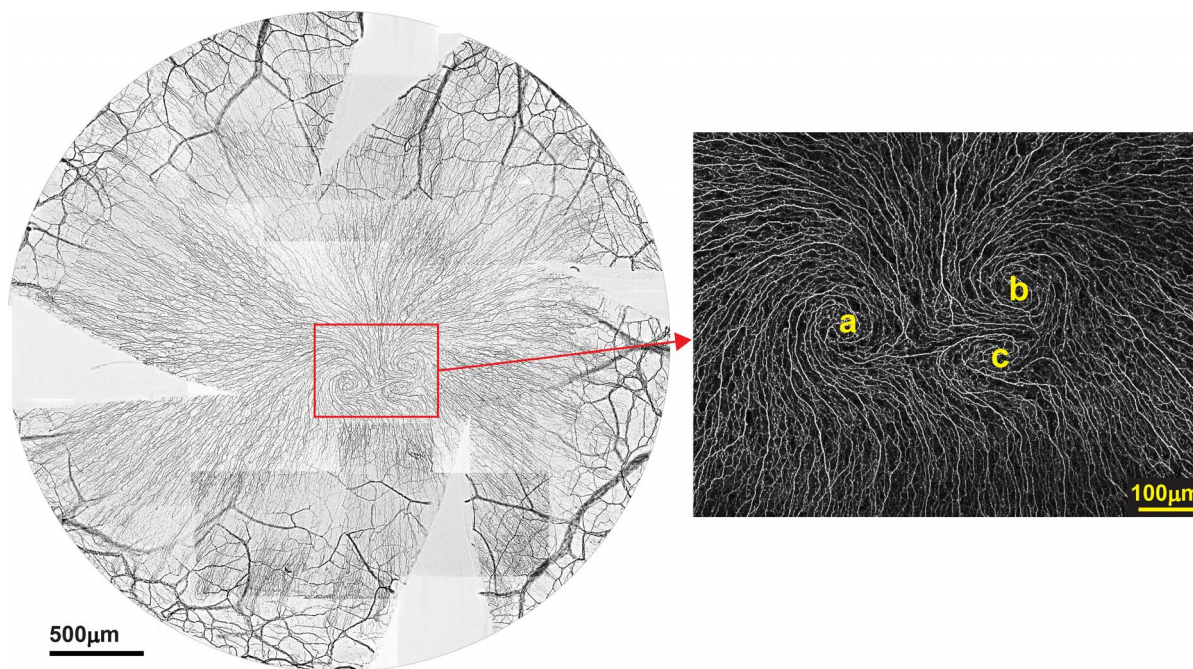


FIGURE 4. Whole-mount view of entire subbasal nerves in a cornea with three vortices labeled with β III-tubulin antibody. The highlighted image shows the details of the three vortices in which vortices *a* and *c* go clockwise, while vortex *b* goes counterclockwise.

(62% \pm 1%) than the percentage of SP-positive terminals (59.3% \pm 0.8%; $P < 0.05$). Similarly, in the main stromal trunks recorded within the limbus, CGRP-positive nerve bundles were more abundant (57% \pm 1.2%) than the SP-positive nerve bundles 51.2% \pm 1.6%, ($n = 5$ eyes; $P < 0.05$).

CGRP- and SP-Positive Neurons in the Trigeminal Ganglion

To investigate the origin and relative contents of the sensory neuropeptides CGRP and SP in neurons of the TG, cross-sections were double stained with β III-tubulin. As shown in Figure 8A, 31.9% \pm 1.2% of the total neurons were CGRP

positive while 26.2% \pm 0.9% were SP-positive neurons. ($n = 10$ mice, $P < 0.005$). Images in Figures 8B and 8C show neurons labeled with each neuropeptide. Double immunofluorescence with CGRP and SP antibodies (Fig. 8D) demonstrate that all SP-positive neurons were also CGRP-positive, while there were some CGRP-positive neurons that were negative for SP.

DISCUSSION

We used a modified technique of immunofluorescence and imaging to show, for the first time, the entire mouse corneal

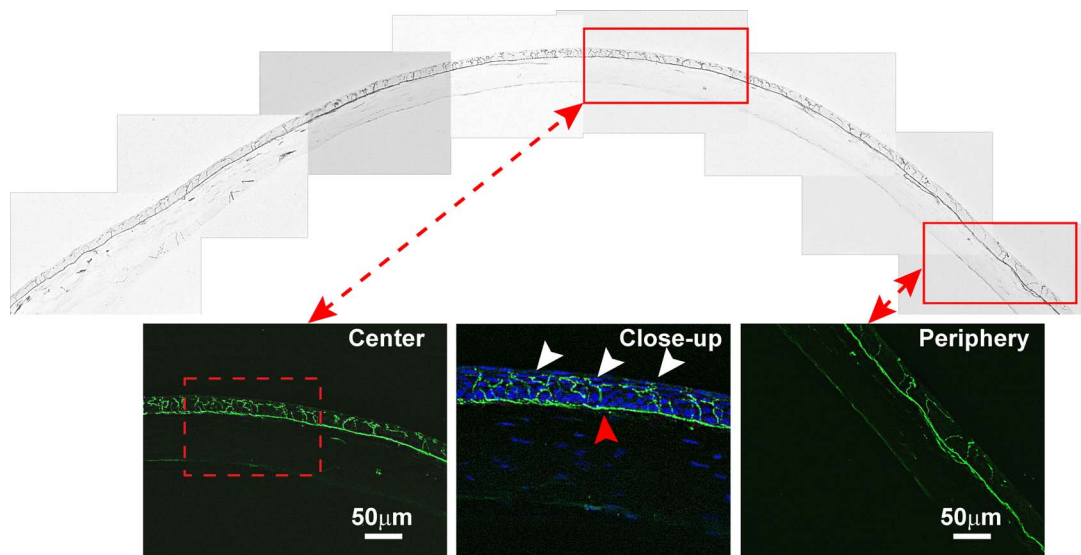


FIGURE 5. Entire cross-sectional view of mouse corneal innervation labeled with β III-tubulin antibody. Highlighted images show the detailed distribution of epithelial terminals at the center and periphery. A close-up image counterstained with DAPI shows the location of subbasal bundles (red arrow) and the shape of epithelial terminals (white arrows).

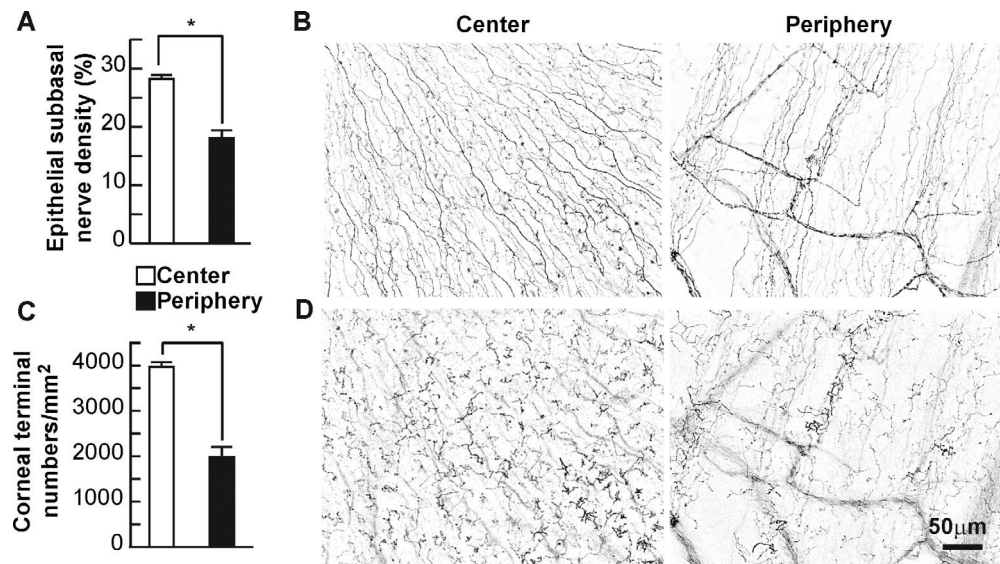


FIGURE 6. Difference of corneal subbasal nerve density and nerve terminals between the central and the peripheral zones. (A) Nerve density in mouse corneas was calculated as the percentage of the total area in each image. A total of 160 images (80 images/zone) recorded with a $\times 20$ objective lens from 10 corneas (male/female = 5/5 corneas) were used. Data expressed as average \pm SEM. $*P < 0.001$. (B) Representative images of central and peripheral subbasal nerves. (C) Number of epithelial nerve terminals; 48 images (24 images/zone) from 6 corneas were used. The number of terminals was counted per millimeter squared. Data expressed as average \pm SEM. $*P < 0.001$. (D) Representative images of nerve terminals recorded from the central and peripheral zones of the same cornea.

nerve architecture including the nerve terminals, subbasal nerve bundles, and stromal nerve trunks.

We found that in very young mice (1–3 weeks after birth), the cornea present a dense network of stromal nerves but that the epithelial nerve fibers that budded from the network are short, thin, and extend without a given direction. Previous work using C57/B6 mice of 10 days and 4 weeks had shown a similar pattern in the central cornea.¹⁵ Those nerve fibers gradually grow with the maturity of the mice, and a well-defined whorl-like structure appears at 4 weeks. From 4 to 6 weeks, the subbasal nerve bundles become longer and denser. The cornea size increases with aging. As we measured in this study, the radius increases approximately 2.6 times from newborn mice (average: 0.58 mm) to adult mice (average: 1.5 mm). Therefore, it is possible that a correlation exists between the length of the subbasal nerve bundles and the changes in corneal size as associated with the age of the mouse. At 8 weeks, the corneal nerves reach maturity with stromal nerves originating from four major trunks and fewer stromal nerves in the central cornea. The mechanism of stromal nerve regression when the mouse reaches maturity is unknown. One possibility is that there is a decreased release of growth factors from stromal keratocytes. Early studies suggested there is cross-talk between the nerves and corneal resident cells.^{29,30} During postnatal eye development, corneal epithelial and stromal cells secrete growth factors—such as nerve growth factor,^{6,31,32} ciliary neurotrophic factor,³³ glial cell line-derived neurotrophic factor,^{34,35} vascular endothelial growth factor,³⁶ and pigment epithelium derived factor³⁷—that may influence nerve fiber extension and survival. Very young mouse corneas have a high density of keratocytes that decrease by age 12 days and change from active to quiescent keratocytes in normal adult corneas.³⁸ This low metabolism may be unable to produce enough growth factors to support the survival of the dense stromal nerves in the central cornea observed at a young age.

The mouse is considered to be an adult at 8 weeks³⁹; however, in our experiments no noticeable changes in the nerve architecture were found up to 24 weeks. These results are in agreement with a recent study using “in vivo” confocal

microscopy reporting that mouse subbasal nerve density is constant from age 8 to 52 weeks.³³ We found that corneal innervation in adult mice share many common features with humans.²⁵ The epithelial nerve bundles derived from the peripheral stromal branches ran centripetally and converged to form the whorl-like structure or vortex at the central cornea. The density of stromal nerves are lower in the center than in the periphery, while the density of epithelial nerves including the subbasal nerves and free endings are significantly higher in the center than in the periphery. We also observed that there is no difference between male and female mice. However, there are some features in mouse corneal innervation that we have not found in humans. In human corneas, although the patterns and locations of the vortex differ among the samples, every cornea analyzed has only one vortex; in mice, we found that 18% of the corneas have more than one whorl-like structure per cornea. Early studies have postulated that the combined effect of the electric and magnetic fields on centripetally migrating epithelial cells lead to a clockwise converged pattern, and it is likely that similar effects are exerted on corneal subbasal nerves.^{14,40} However, this theory cannot explain the phenomenon of counterclockwise pattern and the finding that some corneas show two vortexes running in opposing directions. Hence, a more reasonable explanation is needed.

Another difference found was that mature mice corneas have higher epithelial nerve density than humans. Compared with human corneas aged 40 to 57 years,²⁵ there was a $28.2\% \pm 2.54\%$ nerve density in the mouse central area versus an $18.8\% \pm 2.1\%$ in humans, and an $18.1\% \pm 3.2\%$ vs. $11.1\% \pm 2.3\%$ in the peripheral area. Coincidentally, the number of terminals/mm² of corneal epithelia was also greater in mice (center, 3972 ± 284 ; periphery, 1976 ± 487) than in humans (center, 525 ± 72 ; periphery, 230 ± 46). Although the reasons for this difference are unknown, we agree with Yu and Rosenblatt²⁰ that a higher density of epithelial innervation may be needed by either anatomic or functional requirements specific to the mouse.

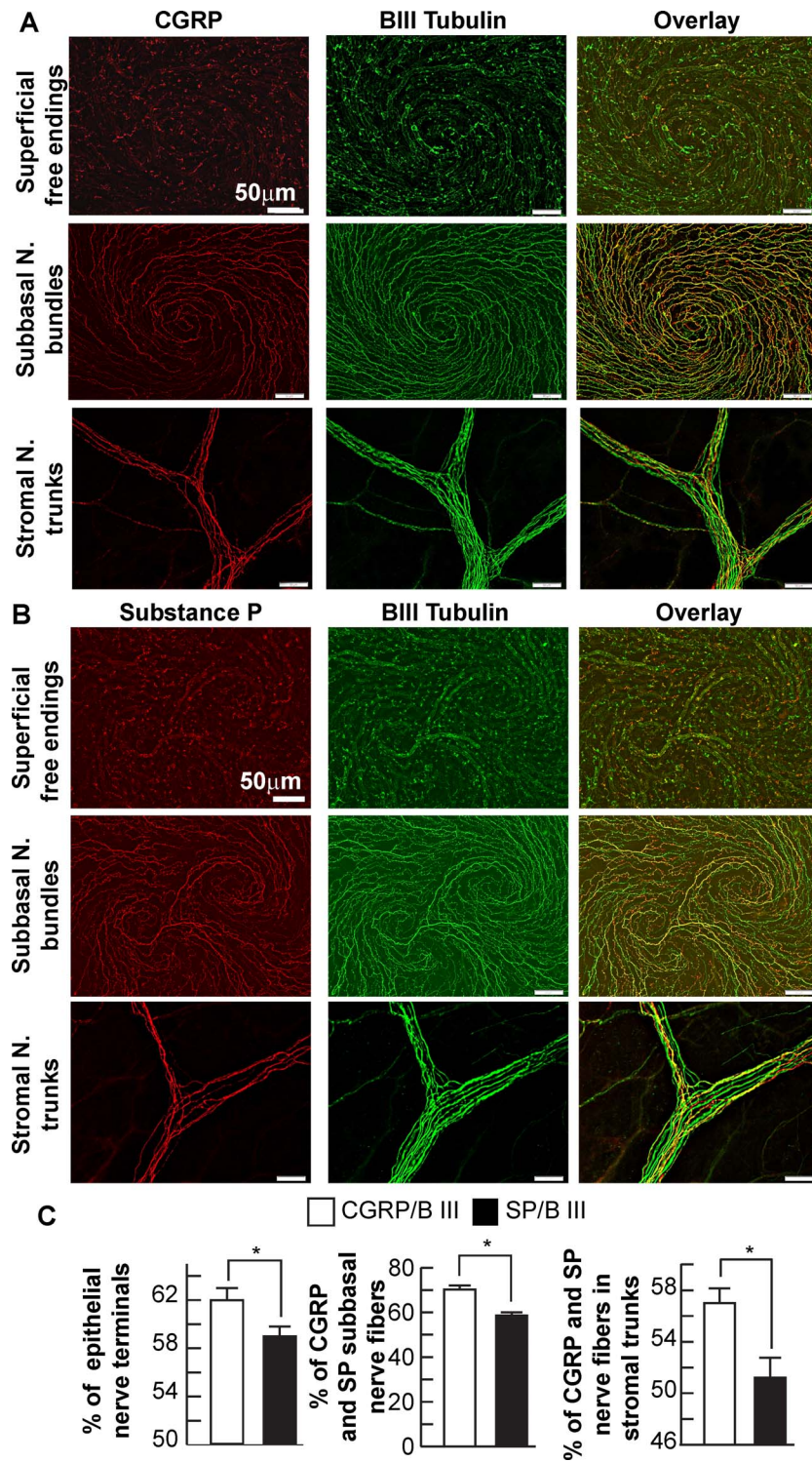


FIGURE 7. The relative content of sensory neuropeptides in mouse corneas. (A, B) Representative images showing the expression of CGRP- and SP-positive nerves in the central subbasal nerve bundles, terminals, and limbal stromal trunks. (C) Percentage calculated as ratios of CGRP- or SP-positive nerves versus total nerve area (β III-tubulin nerves) in each image. A total of 24 images for each neuropeptide and the same number of images for β III-tubulin were recorded from six corneas. Data expressed as average \pm SEM. * $P < 0.001$.

Sensory nerves originating from the TG innervate ocular tissues, including the cornea and iris,⁴¹⁻⁴³ and loss of corneal sensory innervation can result in morphologic and metabolic epithelial disturbance. The expression of the sensory neuropeptides CGRP and SP in the corneas has been studied previously by both histochemical and immunofluorescence

methods in a wide range of animal species,⁴³⁻⁴⁹ but their distribution in the entire tissue and their relative content in mouse corneas was not investigated. In the current study, we used double-labeling immunofluorescence to study the relative contents of these neuropeptides. Our results showed that the corneas contain a large number of CGRP- and SP-positive nerve

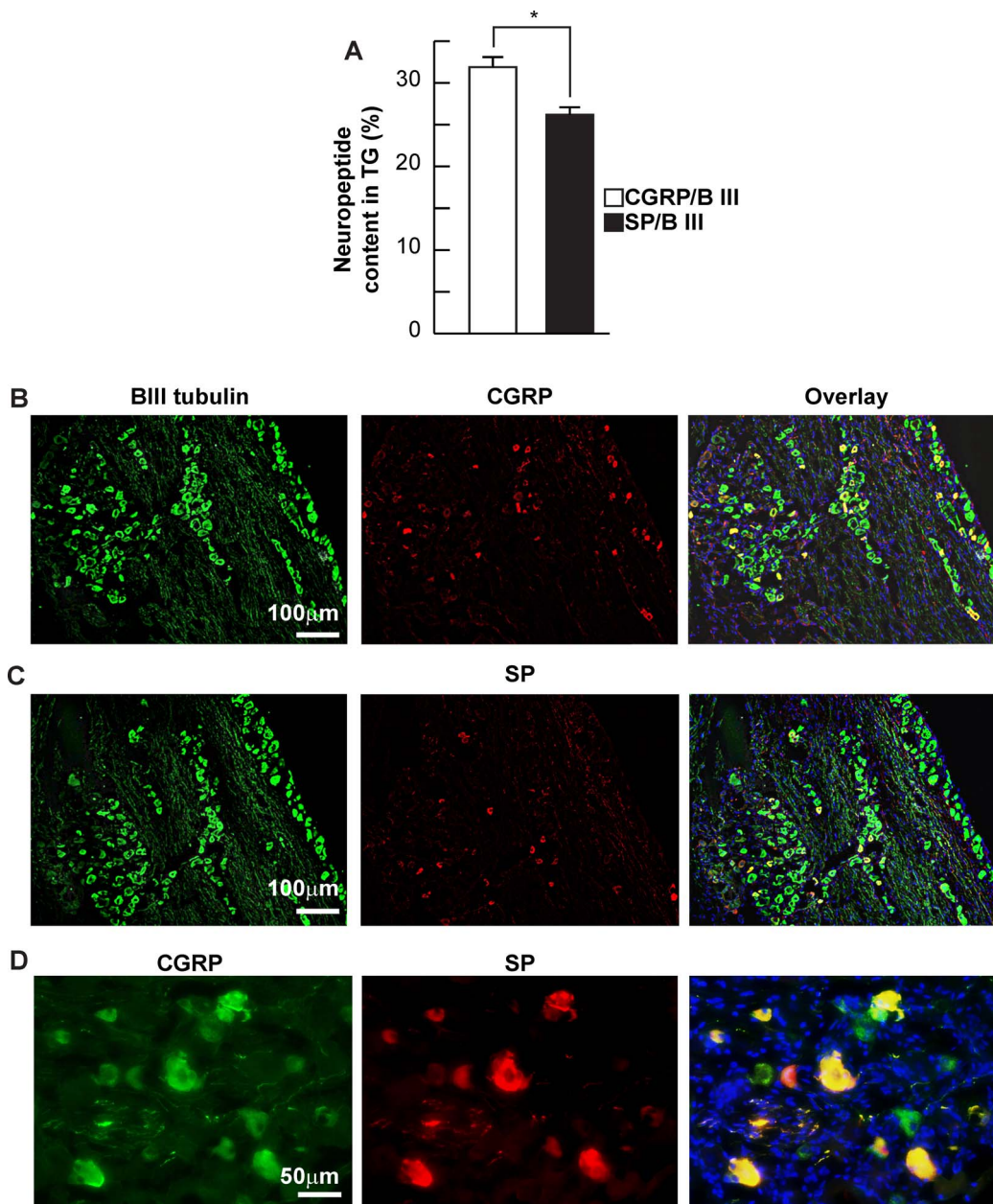


FIGURE 8. Double labeling of sensory neuropeptides in mouse trigeminal ganglion. **(A)** Relative density of CGRP- or SP-positive neurons. For each neuropeptide, 20 sections randomly selected from 5 mice were counted in a blind fashion. Data represent the average ratios (mean \pm SEM) of CGRP- or SP-positive cells versus β III-tubulin neurons. $*P < 0.01$. **(B, C)** Representative images. **(D)** Colocalization of CGRP- and SP-positive neurons.

fibers. These two main sensory neuropeptides have been shown to induce epithelial cell proliferation, migration, and adhesion, facilitating corneal wound healing.⁵⁰⁻⁵² They are involved in the regulation of tear production and mucus secretion from goblet cells⁵³ and participate in the irritative and allergic response of the ocular surface.⁵⁴

Comparison of the proportions of CGRP- with SP-positive fibers shows that the content of CGRP is higher than that of SP in both epithelial and stromal innervation. This result is in agreement with our previous findings in the rabbit model in which the proportion of CGRP is significantly higher than that of SP-positive fibers in the corneal and iris innervations.^{8,28} An early study in the canine model has reported that both CGRP- and SP-positive nerve fibers take up 99% of the total

corneal innervation.⁴⁹ This result is much higher than those we have found in the rabbit and mouse corneas. The discrepancies may be due to the difference between the animal species, rather than the techniques of assessment used in the studies.

The sensory nerves, which innervate the cornea and iris, mainly originate from the ophthalmic division of the trigeminal nerve, with a very small amount deriving from the superior cervical ganglion and ciliary ganglion.⁵⁵⁻⁵⁷ In a recent study, we have reported that in the rabbit TG, the number of CGRP-positive neurons significantly outnumber SP-positive neurons, which are also labeled with CGRP.²⁸ Similar results were found in the mouse TG. Our results are also in agreement with earlier studies in the rat and guinea pig,^{58,59} suggesting that those

species share a similar expression pattern of sensory neuro-peptides in the TG.

In summary, using a modified technique of immunofluorescence and imaging, we provided a complete map of the entire nerve architecture and the total sensory neuropeptide distribution of the mouse cornea. The finding that the mouse corneal innervation has many similarities to human cornea makes the mouse an appropriate model to study pathologies in which corneal nerves are involved.

Acknowledgments

Supported by National Eye Institute Grant R01 EY19465, National Institutes of Health/National Institute of General Medical Sciences Grant P30GM103340, and a grant from the Research Foundation to Prevent Blindness.

Disclosure: **J. He**, None; **H.E.P. Bazan**, None

References

1. Beuerman RW, Schimmelpfening B. Sensory denervation of rabbit cornea affects epithelial properties. *Exp Neurol*. 1980; 69:196-201.
2. Garcia-Hirschfeld J, Lopez-Briones LG, Belmonte C. Neurotrophic influences on corneal epithelial cells. *Exp Eye Res*. 1994;59:597-605.
3. Müller LJ, Marfurt CF, Kruse F, Tervo TMT. Corneal nerves: structure, contents and function. *Ex Eye Res*. 2003;76:521-542.
4. Belmonte C, Acosta MC, Gallar J. Neural basis of sensation in intact and injured corneas. *Exp Eye Res*. 2004;78:513-525.
5. Shaheen BS, Bakir M, Jain S. Corneal nerves in health and disease. *Surv Ophthalmol*. 2014;59:263-285.
6. Esquenazi S, Bazan HEP, Bui V, He J, Kim DB, Bazan NG. Topical combination of NGF and DHA increases rabbit corneal generation after PRK. *Invest Ophthalmol Vis Sci*. 2005;46: 3121-3127.
7. Cortina MS, He J, Li N, Bazan NG, Bazan HEP. Neuroprotectin D1 synthesis and corneal nerve regeneration after experimental surgery and treatment with PEDF plus DHA. *Invest Ophthalmol Vis Sci*. 2010;51:804-810.
8. Cortina MS, He J, Li N, Bazan NG, Bazan HEP. Recovery of corneal sensitivity, CGRP positive nerves and increased wound healing are induced by PEDF plus DHA after experimental surgery. *Arch Ophthalmol*. 2012;130:76-83.
9. Cortina MS, He J, Russ T, Bazan NG, Bazan HEP. Neuroprotectin D1 (NPD1) restores corneal nerve integrity and function after damage from experimental surgery. *Invest Ophthalmol Vis Sci*. 2013;54:4109-4116.
10. He J, Cortina MS, Kakazu Azucena H, Bazan HEP. The PEDF neuroprotective domain plus DHA selectively induces corneal nerve regeneration after experimental surgery. *Invest Ophthalmol Vis Sci*. 2015;56:3505-3513.
11. Dvorscak L, Marfurt CF. Age-related changes in rat corneal epithelial nerve density. *Invest Ophthalmol Vis Sci*. 2008;49: 910-916.
12. Ivanusic JJ, Wood RJ, Brock JA. Sensory and sympathetic innervation of the mouse and guinea pig corneal epithelium. *J Comp Neurol*. 2013;521:877-893.
13. De Castro F, Silos-Santiago I, López de Armentia M, Barbacid M, Belmonte C. Corneal innervation and sensitivity to noxious stimuli in trkA knockout mice. *Eur J Neurosci*. 1998;10:146-152.
14. Leiper IJ, Ou J, Walczysko P, et al. Control of patterns of corneal innervation by Pax6. *Invest Ophthalmol Vis Sci*. 2009; 50:1122-1128.
15. McKenna CC, Lwigale PY. Innervation of the mouse cornea during development. *Invest Ophthalmol Vis Sci*. 2011;52:30-35.
16. Wang C, Fu T, Xia C, Li Z. Changes in mouse corneal epithelial innervation with age. *Invest Ophthalmol Vis Sci*. 2012;53: 5077-5084.
17. Puk O, Dalke C, Favor J, de Angelis MH, Graw J. Variations in eye size parameters among different strains of mice. *Mamm Genome*. 2006;17:851-857.
18. Yun H, Rowe AM, Lathrop KL, Harvey SA, Hendricks RL. Reversible nerve damage and corneal pathology in murine herpes simplex stromal keratitis. *J Virol*. 2014;88:7870-7880.
19. Cai D, Zhu M, Petroll WM, Koppaka V, Robertson DM. The impact of type 1 diabetes mellitus on corneal epithelial nerve morphology and the corneal epithelium. *Am J Pathol*. 2014; 184:2662-2670.
20. Yu CQ, Rosenblatt MI. Transgenic corneal neurofluorescence in mice: a new model for in vivo investigation of nerve structure and regeneration. *Invest Ophthalmol Vis Sci*. 2007; 48:1535-1542.
21. Namavari A, Chaudhary S, Sarkar J. In vivo serial imaging of regenerating corneal nerves after surgical transection in transgenic thyl-YFP mice. *Invest Ophthalmol Vis Sci*. 2011; 52:8025-8032.
22. Yan Y, Sun HH, Mackinnon SE, Johnson PJ. Evaluation of peripheral nerve regeneration via in vivo serial transcutaneous imaging using transgenic Thy1-YFP mice. *Exp Neurol*. 2011; 232:7-14.
23. Chaudhary S, Namavari A, Yco L, et al. Neurotrophins and nerve regeneration-associated genes are expressed in the cornea after lamellar flap surgery. *Cornea*. 2012;31:1460-1467.
24. He J, Bazan HEP. Omega-3 fatty acids in dry eye and corneal nerve regeneration after refractive surgery. *Prostaglandins Leukot Essent Fatty Acids*. 2010;82:319-325.
25. He J, Bazan NG, Bazan HEP. Mapping the entire human corneal nerve architecture. *Exp Eye Res*. 2010;91:513-523.
26. He J, Bazan HEP. Mapping the nerve architecture of diabetic human corneas. *Ophthalmology*. 2012;119:956-964.
27. He J, Bazan HEP. Corneal nerve architecture in a donor with unilateral corneal epithelial basement membrane dystrophy. *Ophthalmic Res*. 2013;49:185-191.
28. He J, Bazan HEP. Morphology and neurochemistry of rabbit iris innervation. *Exp Eye Res*. 2015;135:182-191.
29. Chan KY, Jones RR, Bark DH, Swift J, Parker JA, Haschke RH. Release of neurotrophic factor from rabbit corneal epithelium during wound healing and nerve regeneration. *Exp Eye Res*. 1987;45:633-646.
30. Kubilus JK, Linsenmayer TF. Developmental corneal innervation: interactions between nerves and specialized apical corneal epithelial cells. *Invest Ophthalmol Vis Sci*. 2010;51: 782-789.
31. Lambiasi A, Manni L, Rama P, Bonini S. Clinical application of nerve growth factor on human corneal ulcer. *Arch Ital Biol*. 2003;141:141-148.
32. Chen L, Wei RH, Tan DT, Beuerman RW, Li W, Zhao S. Nerve growth factor expression and nerve regeneration in monkey corneas after LASIK. *J Refract Surg*. 2014;30:134-139.
33. Reichard M, Hovakimyan M, Guthoff RF, Stachs O. In vivo visualisation of murine corneal nerve fibre regeneration in response to ciliary neurotrophic factor. *Exp Eye Res*. 2014; 120:20-27.
34. You L, Kruse FE, Völcker HE. Neurotrophic factors in the human cornea. *Invest Ophthalmol Vis Sci*. 2000;41:692-702.
35. Qi H, Chuang EY, Yoon KC, et al. Patterned expression of neurotrophic factors and receptors in human limbal and corneal regions. *Mol Vis*. 2007;13:1934-1941.

36. Li Z, Burns AR, Han L, Rumbaut RE, Smith CW. IL-17 and VEGF are necessary for efficient corneal nerve regeneration. *Am J Pathol.* 2011;178:1106-1116.
37. Karakousis PC, John SK, Behling KC, et al. Localization of pigment epithelium derived factor (PEDF) in developing and adult human ocular tissues. *Mol Vis.* 2001;7:154-163.
38. Song J, Lee YG, Houston J, et al. Neonatal corneal stroma development in the normal and lumican-deficient mouse. *Invest Ophthalmol Vis Sci.* 2003;44:548-557.
39. Hanlon SD, Patel NB, Burns AR. Assessment of postnatal corneal development in the C57BL/6 mouse using spectral domain optical coherence tomography and microwave-assisted histology. *Exp Eye Res.* 2011;93:363-370.
40. Dua HS, Singh A, Gomes JA, Laibson PR, Donoso LA, Tyagi S. Vortex or whorl formation of cultured human corneal epithelial cells induced by magnetic fields. *Eye.* 1996;10:447-450.
41. Miller A, Costa M, Furness JB, Chubb IW. Substance P immunoreactive sensory nerves supply the rat iris and cornea. *Neurosci Lett.* 1981;23:243-249.
42. Shamir MH, Ofri R. Comparative neuro-ophthalmology. In: Gelatt KN, ed. *Essentials of Veterinary Ophthalmology*. 2nd ed. Ames, IA: Wiley-Blackwell; 2008:451.
43. Jones MA, Marfurt CF. Calcitonin gene-related peptide and corneal innervation: a developmental study in the rat. *J Comp Neurol.* 1991;313:132-150.
44. Uusitalo H, Krootila K, Palkama A. Calcitonin gene-related peptide (CGRP) immunoreactive sensory nerves in the human and guinea pig uvea and cornea. *Exp Eye Res.* 1989;48:467.
45. Kuwayama Y, Stone RA. Distinct substance P and calcitonin gene-related peptide immunoreactive nerves in the guinea pig eye. *Invest Ophthalmol Vis Sci.* 1987;28:1947-1954.
46. Tervo K, Tervo T, Eränkö L, Eränkö O. Substance P immunoreactive nerves in the rodent cornea. *Neurosci Lett.* 1981;25:95-97.
47. Oksala O, Stjernschantz J. Effects of calcitonin gene-related peptide in the eye: a study in rabbits and cats. *Invest Ophthalmol Vis Sci.* 1988;29:1006.
48. Terenghi G, Polak JM, Ghatei MA, et al. Distribution and origin of calcitonin gene-related peptide (CGRP) immune reactivity in the sensory innervation of the mammalian eye. *J Comp Neurol.* 1985;233:506-516.
49. Marfurt C, Murphy C, Floraczek JL. Morphology and neurochemistry of canine corneal innervation. *Invest Ophthalmol Vis Sci.* 2001;42:2242-2251.
50. Mikulec AA, Tanelian DL. CGRP increases the rate of corneal re-epithelialization in an in vitro whole mount preparation. *J Ocul Pharmacol Ther.* 1996;12:417-423.
51. Yang L, Di G, Qi X, et al. Substance P promotes diabetic corneal epithelial wound healing through molecular mechanisms mediated via the neurokinin-1 receptor. *Diabetes.* 2014;63:4262-4274.
52. Murphy CJ, Marfurt CF, McDermott A, et al. Spontaneous chronic corneal epithelial defects in dogs: clinical features, innervation and effect of topical SP with or without IGF-1. *Invest Ophthalmol Vis Sci.* 2001;42:2252-2261.
53. Kovocs I, Ludany A, Koszegi T, et al. Substance P release from sensory nerve endings influences tear secretion and goblet cell function in the rat. *Neuropeptides.* 2005;39:395-402.
54. Sacchetti M, Micera A, Lambiase A, et al. Tear levels of neuropeptides increase after specific allergen challenge in allergic conjunctivitis. *Mol Vis.* 2011;17:47-52.
55. Gurusinge CJ, Bell C. Substance P immunoreactivity in the superior cervical ganglia of normotensive and genetically hypertensive rats. *J Auton Nerv Syst.* 1989;27:249-56.
56. Kuwayama Y, Stone RA. Distinct substance P and calcitonin gene-related peptide immunoreactive nerves in the guinea pig eye. *Invest Ophthalmol Vis Sci.* 1987;28:1947-1954.
57. Grimes PA, Koeberlein B, Tigges M, Stone RA. Neuropeptide Y-like immunoreactivity localizes to preganglionic axon terminals in the Rhesus monkey ciliary ganglion. *Invest Ophthalmol Vis Sci.* 1998;39:227-232.
58. Lee Y, Kawai Y, Shiosaka S, et al. Coexistence of calcitonin gene-related peptide and substance P-like peptide in single cells of the trigeminal ganglion of the rat: immunohistochemical analysis. *Brain Res.* 1985;330:194-196.
59. Kuwayama Y, Terenghi G, Polak JM, Trojanowski JQ, Stone RA. A quantitative correlation of substance P-, calcitonin gene-related peptide- and cholecystokinin-like immunoreactivity with retrogradely labeled trigeminal ganglion cells innervating the eye. *Brain Res.* 1987;405:220.